13th International Symposium on Turbulence and Shear Flow Phenomena (TSFP13)
Montreal, Canada, June 25–28, 2024

PREDICTING THE GLOBAL DRAG OF TURBULENT FLOW OVER ROUGHNESS STRIPS

Jonathan Neuhauser, Davide Gatti, Carola Schmidt, Bettina Frohnapfel
Institute of Fluid Mechanics
Karlsruhe Institute of Technology
Kaiserstr. 12, 76131 Karlsruhe, Germany
jonathan.neuhauser|davide.gatti|carola.schmidt|bettina.frohnapfel@kit.edu

ABSTRACT

Predicting the global drag of heterogeneous rough surfaces remains one of the great challenges in roughness research (Chung et al., 2021). In the limit where patch sizes are much larger than the boundary layer thickness, predictive formulas can be derived under the assumption that the flow is in local equilibrium with the surface properties (Neuhauser et al., 2022; Hutchins et al., 2023). The present work extends this concept to predict the drag behaviour of surfaces with spanwise heterogeneous roughness properties which vary over length scales comparable to the boundary layer thickness. The drag predictions are compared with high fidelity measurements obtained in an air channel flow facility (Frohnapfel et al., 2024).

MOTIVATION AND APPROACH

Drag predictions for flows over rough surfaces rely on the prescription of a homogeneous roughness length scale; i.e. an equivalent sandgrain roughness k_s. This quantity is typically obtained empirically from drag measurements (physical experiments or numerical experiments based on DNS), through existing correlations with statistical surface properties (Chung et al., 2021) or recently also based on data driven approaches. In the fully rough flow regime, when the friction coefficient C_f is independent of the Reynolds number, k_s is directly related to the roughness function ΔU^+ through

$$\Delta U^+ = \frac{1}{\kappa} \ln k_s^+ + B - 8.5 \tag{1}$$

which represents a downward shift in the logarithmic region of the viscous scaled mean-velocity profile. This shift can be introduced into RANS-based full scale drag predictions.

For inhomogeneous surfaces, modelling the influence of the roughness on the drag behavior is more difficult. In particular, a fully rough behavior might not be obtained even at high Re. We consider the often-studied case of surface properties that are piecewise constant in the spanwise direction and independent of the streamwise direction (Chung et al., 2021). For this case, we have a high-quality experimental data set from our turbulent channel flow facility (Frohnapfel et al., 2024). The considered surfaces consist of streamwise aligned roughness strips (P60 sandpaper) which alternate with smooth surface parts of the same width where the width is set to $s \approx \delta$ and $s \approx 2\delta$. The data set contains $C_f(Re_b)$ for these strip type surfaces and the homogeneous rough and smooth reference cases over a Reynolds number range $4500 < Re_b < 85000$. This data does not indicate a fully rough behaviour for the roughness strips within the considered Reynolds number range. However, there is an intermediate Reynolds number range in which the data appear to remain at a constant C_f similar to a fully-rough behaviour before dropping again to lower values. The measurement data can be seen in Fig. 5 at the end of this manuscript (thick symbols). The question at hand is whether the observed $C_f(Re_b)$ relation for rough strips can be predicted based on $C_f(Re_b)$ for the homogeneous rough and homogeneous smooth surfaces.

An equilibrium assumption (the flow is in local equilibrium with the boundary condition above each strip) leads to the suggestion of a power mean average for C_f (Neuhauser et al., 2022; Hutchins et al., 2023) valid for very large spanwise wavelength (relative to the boundary layer height δ) of the roughness inhomogeneity; i.e. very wide strips. At present, it remains unknown what defines the lower limit of this 'very large' wavelength. The patch sizes often considered in experiments and simulations are in the order of δ such that the equilibrium assumption is obviously not valid. It is unclear how to include this effect in predictions.

The present analysis is prompted by two particular observations in the aforementioned data set:

1. Both spanwise wavelengths considered have a 50% surface coverage but the global drag is lower for larger s.
2. The power mean underestimates the drag for both s and all Reynolds numbers, particularly for high $\mathrm{Re_b}$. As the power mean is derived in the limit of infinite strip size, this is consistent with the observed trend of reduced global drag for larger s.

In this contribution, we explore a new modelling approach based on the idea of hydraulic channel height. In geology, 'hydraulic aperture' is defined as the height of a smooth-walled channel that yields the same flow rate for a given pressure gradient as the rough-walled conduit (Zimmerman and Bodvarsson, 1996). This concept was extended to turbulent flows in von Deyn et al. (2022) and Frohnapfel et al. (2024) - a rough-walled channel reduces the flow rate at a given pressure gradient, and thus has a lower hydraulic channel height (which is a function of k_s and Re_b). The present roughness (P60 sandpaper), for example, corresponds to approx. 10% (30%) hydraulic reduction of channel height at $\mathrm{Re_b} = 1 \times 10^4$ (8×10^4) in our channel flow facility if the roughness is placed homogeneously on both channel walls.

This observation is used to construct a modelling approach for the global friction coefficient of surfaces with

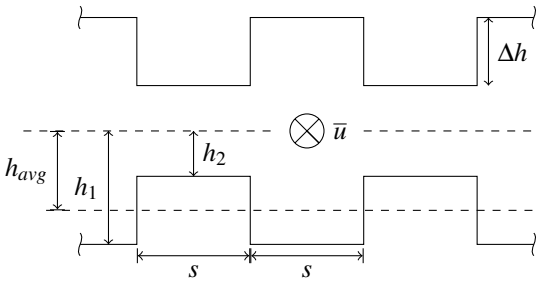

Figure 1: Sketch of the spanwise periodic ridge-type setup. Mean flow direction is perpendicular to the drawing plane.

streamwise aligned roughness strips. We postulate that the resulting global drag change related to the transition region between rough and smooth equilibrium conditions can be estimated based on channel flow simulations in which the reduced hydraulic channel height over the rough strip (observed under turbulent flow conditions) is represented by a geometric reduction of the channel height. The channel with rough strips is thus modelled by a geometry with periodically arranged ridges oriented in the streamwise direction as depicted in Fig 1. The global drag behaviour of the flow in the structured channel with ridges compared to its theoretical limit for very wide ridges is considered under laminar and turbulent conditions. Eventually, it is shown that the easy-to-obtain laminar results for the structured channel can be used to derive a correction for the power mean average of C_f which was previously observed to under-predict the measurement results for the turbulent channel flow with streamwise aligned (non-elevating) roughness strips.

In the following, we refer to the global skin friction coefficient in case of a spanwise inhomogeneous geometry and the related quantities with an overbar (as introduced in the next section), whereas global quantities for homogeneous surfaces are written without overbar.

RESULTS

Skin friction coefficient for streamwise-aligned ridges

We aim to estimate the global skin friction coefficient $\overline{C_f} = 2\overline{u_\tau}^2/\overline{u_b}^2$ (where $\overline{(\cdot)}$ denotes spanwise averaged quantities), expressed in terms of friction velocity and bulk velocity, for a channel with structured walls. It can also be expressed in terms of the mean pressure gradient $\Pi = \frac{\partial\langle p\rangle}{\partial x}$, $\overline{C_f} = 2\Pi\tilde{h}/(\rho\overline{u_b}^2)$ (where $\langle\cdot\rangle$ denotes statistical averaging, and $\tilde{h}$ is a reference height, to be defined later). As discussed in Neuhauser et al. (2022), we postulate that two flows which are both in local equilibrium with their respective boundary condition need to have the same mean streamwise pressure gradient in order to co-exist without a separating wall.

For a laminar channel with spanwise alternating heights h_1 and $h_2 < h_1$ (see Fig. 1), in the limit of $s/h_i \gg 1$ (i.e. the additional surface area of the step and interface transients are negligible), the resulting skin friction coefficient may be computed analytically using the classical Hagen-Poiseuille relation:

$$\overline{C_f} = \frac{12}{\overline{Re_b}} \cdot \frac{\tilde{h}^3}{\frac{1}{2}(h_1^3 + h_2^3)} \quad \text{with} \quad \overline{Re_b} = \frac{\overline{u_b} 2\tilde{h}}{\nu} \tag{2}$$

where $\tilde{h}$ is any reference height (to be defined), and $\overline{u_b}$ is the volumetric flow rate per unit width divided by $\tilde{h}$, thus $\overline{Re_b}$ is independent of the choice of $\tilde{h}$ for known flow rate.

The choice of the reference height is relevant when comparing the skin friction coefficient of different setups, and poorly understanding the influence of the reference height may prompt problematic statements regarding changes in drag. Therefore, we consider different choices for $\tilde{h}$ in the evaluation of $\overline{C_f}$. The corresponding results are shown in fig. 2. All plots show the numerically evaluated $\overline{C_f Re_b}$ for different ridge dimensions. The ridge geometry is characterised by its height $\Delta h = h_2 - h_1$ and its width s/h_1. Three different choices for the reference channel height are considered. The first is the 'empty channel height' $\tilde{h} = h_{empty} = h_1$ (Fig. 2a) and the second is a 'meltdown height' $\tilde{h} = h_{avg} = 1/2(h_1 + h_2)$ (Fig. 2b). The dashed red line in these plots corresponds to the analytical solution of a smooth wall laminar channel flow $\overline{C_f Re_b} = 12$ and the blue dashed line represents the limit for very wide ridges ($s/h_i \gg 1$) according to equation (2). The obtained results in these two plots can easily lead to different conclusions for one and the same numerical results.

Using $\tilde{h} = h_{empty}$ (Fig. 2a) yields an increase in $\overline{C_f}$ with increasing ridge height $\Delta h = h_2 - h_1$, while using $\tilde{h} = h_{avg}$ (b)(Fig. 2b) yields a decrease in $\overline{C_f}$ with increasing ridge height (for the limiting case of $h_2 \to 0$, a 'skin friction reduc-

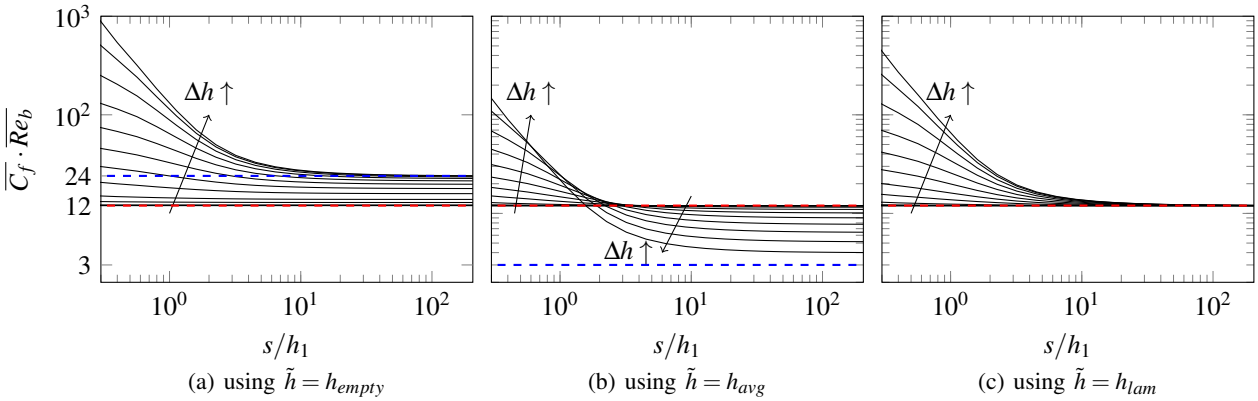

(a) using $\tilde{h} = h_{empty}$ (b) using $\tilde{h} = h_{avg}$ (c) using $\tilde{h} = h_{lam}$

Figure 2: Product of $\overline{Re_b}$ and $\overline{C_f}$ for laminar flow over streamwise-aligned ridges. Displayed are $\Delta h/h_1 = 0.1, 0.2, ..., 0.9$, (dashed red) the value from the canonical laminar relation, $\overline{Re_b} \cdot \overline{C_f} = 12$ and (dashed blue) the $s \to \infty$ asymptote for the case $h_2 \to 0$.

tion' of 75% can be observed)[1].

A third alternative is shown in Fig. 2c). It is introduced to recover the smooth wall solution $\overline{C_f}\overline{Re_b} = 12$ for very wide ridges. Here, the reference channel height is defined as:

$$\tilde{h} = h_{lam} = \sqrt[3]{\frac{1}{2}\left(h_1^3 + h_2^3\right)}, \tag{3}$$

h_{lam} is the height of the (homogeneous smooth-wall) channel that has the same relationship between $\dot{V}$ and $\frac{\partial p}{\partial x}$ as the channel with ridge heights h_1 and h_2, for $s/h_i \gg 1$.

As anticipated $\overline{C_f}$ is independent of the ridge height for the limit of large s when evaluated based on h_{lam} (Fig. 2c) and $\overline{C_f} = 12/\overline{Re_b}$ is recovered in this case. The visible deviation from $\overline{Re_b} \cdot \overline{C_f} = 12$ for smaller strip sizes s/h_1 and large ridge heights $\Delta h/h_1$ stems from the fact that flow is not in local equilibrium. This plot thus provides a measure for the impact of the transition region between the two flow regions on the global drag.

In addition, we observe that for a given pressure gradient, the flow rate per unit width $\dot{V}$ tends towards the equilibrium condition in the thinner part of the channel, but not equally so in the thicker part of the channel (since $h_1 < h_2 \rightarrow s/h_1 > s/h_2$). Consequently, for a given bulk velocity, the pressure gradient tends towards the homogeneous value in the thicker part of the channel, but not equally so in the thinner part of the channel (thus increasing the pressure gradient). In consequence, for finite ridge widths, the global flow rate for a given pressure gradient is lower than in case of very wide ridges.

In the following, we compare these results to the case of turbulent flow over ridges. Similar to the laminar case, an explicit expression for the case of $s \gg h_i$ can be given based on the correlation of Dean (1978), $C_f = 0.073 Re_b^{-1/4}$. We find

$$\overline{C_f} = 0.073\overline{Re_b}^{-1/4} \frac{\tilde{h}^3}{\left(\frac{1}{2}\left(h_1^{12/7} + h_2^{12/7}\right)\right)^{7/4}} \tag{4}$$

[1]This statement generally also holds for walls that are not shaped like a step function, e.g. Daschiel et al. (2012) reported a 50% 'drag reduction' for a channel with sinusoidal walls at the limit of large wavelengths, where the skin friction is evaluated with h_{avg}.

s/h_1	$\Delta h/h_1$	L_z/h_1	N_{el}	Re_b
—	0	4	153600	8000
1	0.132	4	475200	12000
1	0.25	4	124800	8000
1	0.5	4	110400	8000
2	0.25	4	124800	8000
2	0.5	4	123200	8000
8	0.25	16	499200	8000
8	0.5	16	492800	8000

Table 1: Metadata for discussed turbulent cases.

thus, for the choice of

$$\tilde{h} = h_{turb} = \left(\frac{1}{2}\left(h_1^{12/7} + h_2^{12/7}\right)\right)^{7/12} \tag{5}$$

the Dean relationship between $\overline{C_f}$ and $\overline{Re_b}$ is recovered in the wide-strip limit.

In order to investigate the influence of finite s under turbulent flow conditions, DNS simulations of channel flow with streamwise aligned ridges have been performed for the cases listed in Tab. 1. The employed numerical code is NekRS, a portable version of the spectral element code Nek5000 (Fischer et al., 2022). The simulations were set-up using a body-conform mesh and streamwise periodicity, with streamwise box length $L_x = 4\pi h_1$. Element order $n = 7$ and BDF3 / EXT3 timestepping was used. The simulations were conducted at constant flow rate.

Figure 3 shows the resulting skin friction coefficients for different choices of $\tilde{h}$ in analogy to the laminar results shown in Fig. 2. The smooth wall reference is indicated by a black line in these plots. The coloured markers (orange, green, blue) on the right ordinate of each plot depict the limiting case of very wide ridges for the three considered values of Δh. For increasing s, the computed values for $\overline{C_f}$ clearly decrease towards the respective limiting cases, which collapse onto the smooth wall reference when using h_{turb}. Similar to the laminar results discussed before, a 'skin friction drag reduction'

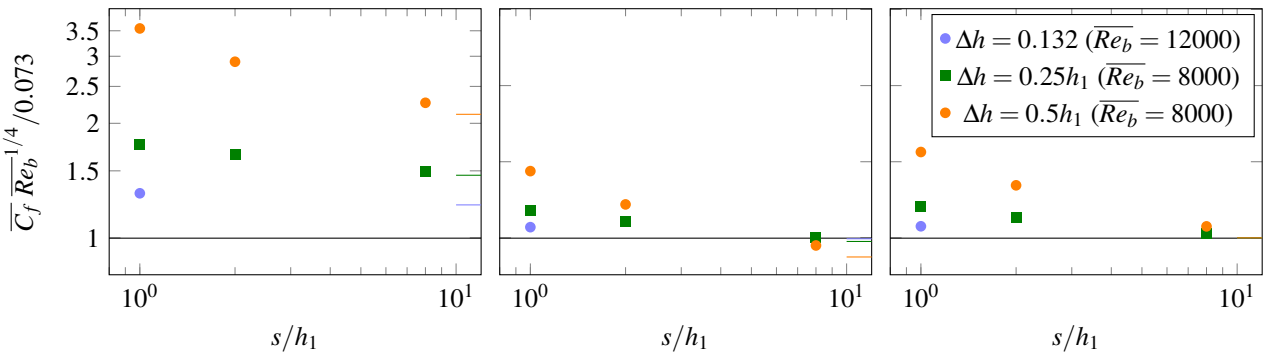

(a) using $\tilde{h} = h_{empty}$ (b) using $\tilde{h} = h_{avg}$ (c) using $\tilde{h} = h_{turb}$

Figure 3: Diagnostic function $\overline{C_f}\ \overline{Re_b}^{1/4}/0.073$ for the considered turbulent cases. Displayed are $\Delta h/h_1 = 0.25$ (green), 0.5 (orange), as well as (lines on the right) the expected value for very large s, evaluated with different definitions for $\tilde{h}$.

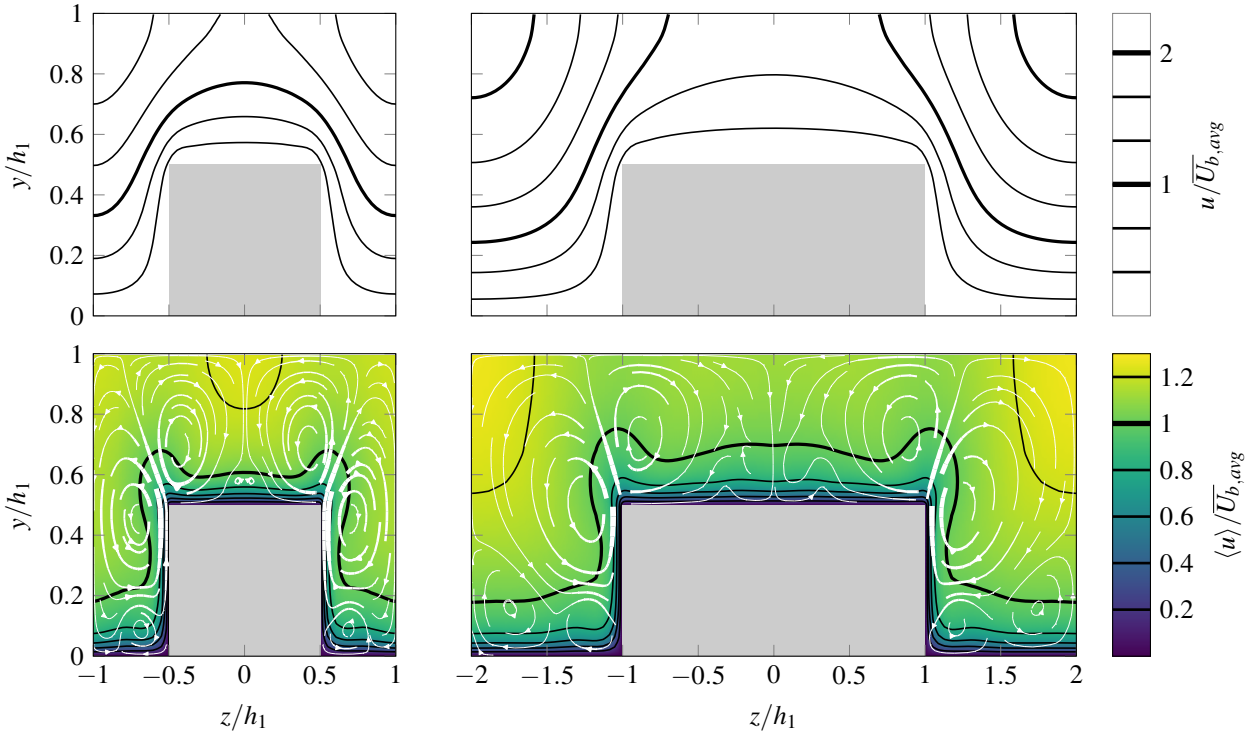

Figure 4: Comparison of laminar (top) and turbulent (bottom) flow over streamwise-aligned ridges for $\Delta h = 0.5h_1$. Left: $s/h_1 = 1$, Right: $s/h_1 = 2$. Top: Laminar flow at constant bulk flow rate, Bottom: Turbulent flow at constant bulk flow rate ($\overline{Re_b} = 8000$). The resulting secondary flow is indicated with streamlines, line thickness of the streamlines indicates magnitude; maximum magnitude is $5.3\%\overline{U_b}_{,avg}$ ($s/h_1 = 0.5$) and $5.5\%\overline{U_b}_{,avg}$ ($s/h_1 = 0.5$).

can be obtained for high s, when evaluating the numerical data using h_{avg}. We note that there is no right or wrong choice for $\tilde{h}$ in the evaluation of C_f. The different choices simply lead to a presentation of the results that are likely to be interpreted differently. For any data evaluation of this type it is thus of utmost importance to communicate how an evaluation of C_f was performed.

For the present study it is important to realise that there is a qualitative similarity between laminar (Fig. 2) and turbulent (Fig. 3) cases, irrespective of the choice of $\tilde{h}$, which suggests that the effect of finite s on $\overline{C_f}$ is mostly a geometric one. This is also supported by closer investigation of the spanwise distribution of streamwise velocity as discussed in the following. Fig. 4 depicts contours of streamwise velocity in part of the channel cross section for the laminar (top) and turbulent (bottom) case for two different ridge widths. We recall that the width of the ridge and of the valley between the ridges is always identical in the present study since the ridges resemble surface roughness that covers 50% of the surface. The velocity contours in the turbulent flow case are significantly more complex than the laminar one since turbulent secondary flow develops in the presence of ridges. This mean flow in the spanwise and wall-normal velocity component is indicated by the white in-plane streamlines Fig. 4 (bottom) which are placed in front of a colour map of the streamwise mean velocity. The turbulent secondary flow clearly impacts the streamwise velocity distribution. Nevertheless, the laminar and turbulent contours of streamwise velocity carry some similarities when one considers the changes that occur with increasing ridge width.

Consider the wall-normal gradient of the streamwise mean velocity (i.e. the local wall shear stress) for $s/h_1 = 1$ (left) and $s/h_1 = 2$ (right). For each flow condition, laminar and turbulent, the wall shear stress distribution on the ridge sides and the ridge top, close to the edge remains very similar when doubling the ridge width. On top of the ridge the flow rate decreases with increasing s (less contours in the laminar case, lower values of $\langle u \rangle$ in the turbulent case) which also results in a reduction of the shear stress in the ridge center. With increasing s there is a flow rate increase above the valley for laminar and turbulent flow which is mostly located further away from the wall while the wall shear stress remains similar. This results in a smaller total wall shear stress for the wider ridge as reflected by the decrease in the diagnostic function ($\overline{Re_b}\overline{C_f}$ for the laminar case, $\overline{Re_b}^{1/4}\overline{C_f}$ for the turbulent case) with increasing s for laminar and turbulent flow conditions.

For the model formulation we rely on the assumption of the same streamwise pressure gradient in different sections (i.e. rough and smooth) of the channel. We can therefore translate the obtained results to a constant pressure gradient scenario. In analogy to the procedure before, we obtain a limiting flow rate that we expect to hold for very wide ridges while the actual flow rate for narrower ridges corresponds to the simulation results. The ratio of actual and expected (limiting) flow rate for laminar and turbulent cases is presented in Tab. 2 in terms of a relative flow rate loss $R_{\dot{V}}$ compared to the limiting case where equilibrium conditions are reached in all parts of the channel. The data show that the relative flow rate loss $R_{\dot{V}}$ increases with larger Δh and smaller s for both, laminar and turbulent flow conditions. As expected $R_{\dot{V}}$ is positive, indicating that the achievable flow rate is lower than the predicted one for idealised equilibrium conditions on smooth and rough patches (modelled through valleys and ridges here). Translating this into $\overline{C_f}$ at a fixed pressure gradient (and thus fixed mean wall shear stress) corresponds to an increase of $\overline{C_f}$ compared to the idealised reference which is in agreement with the experimental observations.

To first approximation, the obtained values for $R_{\dot{V}}$ agree reasonably well for laminar and turbulent flow, which supports the hypothesis that the friction increase due to narrower ridges (i.e. the deviation from the equilibrium state) is mainly a geometric and not a turbulent effect, despite the emergence of strong secondary flow in the turbulent case. Stated differently, the deviation from the limiting equilibrium case is mainly caused by the transients between the subdomains, and those transients and their effect is comparable in magnitude for the laminar and turbulent regime. In addition we note that $R_{\dot{V}}$ is independent of the prescribed pressure gradient (and thus the Reynolds number) in the laminar regime while a (small) Reynolds number dependency is expected for turbulent flow conditions.

s/h_1	$\Delta h/h_1$	$R_{\dot{V}}$ (turbulent)	$R_{\dot{V}}$ (laminar)
1	0.132	0.0393	0.0332
1	0.25	0.1024	0.1125
1	0.5	0.2568	0.3468
2	0.25	0.0679	0.0580
2	0.5	0.1661	0.1837
8	0.25	0.0141	0.0133
8	0.5	0.0390	0.0448

Table 2: Relative flow rate loss $R_{\dot{V}} = 1 - \overline{\dot{V}_{actual}/\dot{V}_{expected,\,limit}}$ for the pressure gradient encountered in the respective simulations in which Re_b was prescribed. Note that for the laminar case, $R_{\dot{V}}$ is independent of pressure gradient or Reynolds number.

Modelling skin friction over spanwise inhomogeneous roughness

In the previous section, we demonstrated a remarkable similarity in the skin friction behaviour of laminar and turbulent flows over streamwise-aligned ridges. Those ridges were considered to represent the reduction of the hydraulic channel height caused by non-protruding roughness strips. In the next step we combine the experimental results obtained for a homogeneously rough channel (these are standard Nikuradse diagram type of data) for the roughness of interest (P60 sandpaper) with the laminar simulation results for ridges to obtain a prediction for the global drag of streamwise aligned roughness strips. For the limiting case of roughness strips with large spanwise dimension and 50% roughness coverage, an estimate of $\overline{C_f}$ may be readily computed from the arithmetic mean of flow rates for the homogeneous smooth and the homogeneous rough case at a given pressure gradient (which is identical to a power mean average for C_f) (Neuhauser et al., 2022). This obtained model prediction is displayed in Fig. 5 as wide-strip limit (brown points). It is purely based on the smooth and rough reference data depicted in black and green in the same plot. The prediction clearly differs from the measurement results for rough strips which are shown by the thick yellow and blue symbols for two different strip widths.

In order to improve the prediction for finite-sized strips, we suggest that the friction behaviour, in particular the spanwise transients before a local equilibrium with the wall boundary condition is reached, is similar to that found in a channel flow with with streamwise-aligned ridges.[2] Due to the dis-

[2]This requires that the additional drag introduced by the ridge side walls doesn't dominate, as is the case for $s \to 0$.

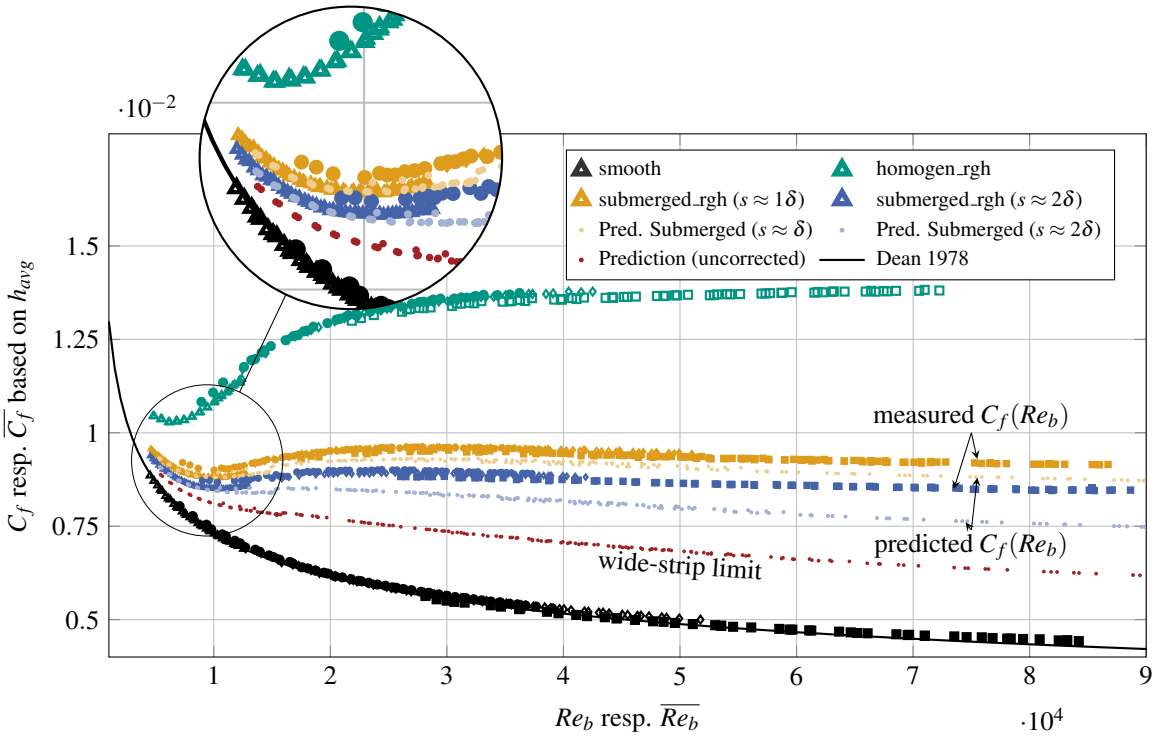

Figure 5: Measurement data from Frohnapfel et al. (2024) (thick symbols for smooth and rough references and roughness strips with two different s) and predictions for the global drag of rough strips (small dots). Different thick symbols within each colour correspond to different flow rate measurement procedures within the experiment which is not in focus here.

cussed similarity between turbulent and laminar data in respect to these transients we rely on the laminar data for the model formulation. The heights h_1 and h_2 correspond to the physical channel height and the hydraulic channel height for the rough channel, respectively.

The predictive model for the global friction coefficient is formulated based on the volume flow rates that can be obtained for a prescribed pressure gradient. For the homogeneous rough and the homogeneous smooth wall, the flow rate for any specific pressure drop is obtained based on the reference data for the channel of height h_1. The arithmetic mean of these two flow rates yields the prediction for the wide-strip limit $\dot{V}_{expected,\ limit}$ as discussed before. This prediction is now corrected using the ratio $\dot{V}_{actual}/\dot{V}_{expected,\ limit}$ from the laminar ridge simulations based on the value of s/h_1 and $\Delta h/h_1$, where Δh is Reynolds number dependent (and roughness-specific). Δh is evaluated based on the homogeneous rough reference data at the same prescribed pressure gradient as used for the prediction of $\dot{V}_{expected,\ limit}$. The corrected volume flow rate at this pressure gradient is used to evaluate a prediction for $\overline{C_f}$ (in which the wall shear stress is defined by the pressure gradient) which yields different results for different strip widths.

Fig. 5 shows the obtained predictions for $\overline{C_f}$ (based on h_{avg}) for two different values of s along with the experimental data, results for the narrower strips are displayed in yellow and for the wider strips in blue. It can clearly be seen that the agreement with experimental data is significantly improved compared to the wide-strip limit (in brown). The new prediction correctly captures the effect of larger C_f for smaller s. Most importantly, the different regimes of the $\overline{C_f}(\overline{Re_b})$-curve are well described by the model. This includes effects at low Re_b (small difference between different values for s since the homogeneous flow rates also differ less), intermediate Re (near-constant C_f over a limited Re range) and high Re_b (decreasing C_f). Based on the model results we expect the appearance of an apparent fully rough condition in an intermediate Reynolds number range to be more pronounced for narrow surface structures and less pronounced for wider ones. Additional measurements for wider roughness strips are presently carried out. We note that the model also correctly captures the qualitative effect that protruding roughness strips (in contrast to the non-protruding ones discussed before) lead to slightly larger values of C_f over the entire Reynolds number regime. The remaining quantitative difference between prediction and measurement results might be partially caused by the presence of turbulent secondary flow at the intersection between different surface parts which is not included in the correction factor obtained from laminar simulations.

SUMMARY AND OUTLOOK

In this paper, we present a framework for predicting C_f for flows over spanwise inhomogeneous surfaces. The surface of interest is composed of spanwise alternating smooth and rough strips in which the roughness does not protrude but is arranged in such a way that its mean height is equivalent to the location of the smooth wall.

For the limit of a surface structure with large strip width, a prediction of $\overline{C_f}$ can be obtained from the $C_f(Re_b)$ behaviour of the comprising surfaces. The underlying assumption is that the flow above each strip is in equilibrium with its boundary conditions. For roughness strips with a width in the order of the boundary layer thickness such a prediction fails. A clear prediction improvement can be obtained when the transients between the equilibrium conditions are included in the model formulation. A simple model for the impact of these transients is obtained by exploiting the drag behaviour of laminar channel flow with streamwise aligned ridges. In this model, the ridge height is deduced from the hydraulic channel height variation of a turbulent flow over rough surfaces as introduced in von Deyn et al. (2022) and Frohnapfel et al. (2024).

The resulting prediction of the global $\overline{C_f}$ for this heterogeneous surface is in very good agreement with measurement data, correctly capturing the difference in global drag for roughness strips of different width with identical roughness coverage (50% of the total surface). Most importantly, the qualitative trend of the friction curve is captured by the model. The structure of the model should allow its applicability to any kind of spanwise heterogeneous roughness, such that the global drag of alternating strips of different roughness size can be predicted. While an improved prediction of the drag behaviour for strip type roughness is an important step forward, we note that the question how to extend the framework to a surface with patchy roughness remains to be addressed in future work.

We greatly acknowledge the support by the German Research Foundation (DFG) under research projects 462658330 and 521110788 and by High Performance Computing Center Stuttgart (HLRS), project ctbctpf.

REFERENCES

D. Chung, N. Hutchins, M. P. Schultz, and K. A. Flack. Predicting the drag of rough surfaces. *Annual Review of Fluid Mechanics*, 53(1):439–471, Jan. 2021.

G. Daschiel, T. Baier, J. Saal, and B. Frohnapfel. On the flow resistance of wide surface structures. *PAMM*, 12(1):569–570, Dec. 2012.

R. B. Dean. Reynolds number dependence of skin friction and other bulk flow variables in two-dimensional rectangular duct flow. *Journal of Fluids Engineering*, 100(2):215–223, June 1978.

P. Fischer, S. Kerkemeier, M. Min, Y.-H. Lan, M. Phillips, T. Rathnayake, E. Merzari, A. Tomboulides, A. Karakus, N. Chalmers, and T. Warburton. NekRS, a GPU-accelerated spectral element Navier–Stokes solver. *Parallel Computing*, 114:102982, Dec. 2022.

B. Frohnapfel, L. von Deyn, J. Yang, J. Neuhauser, A. Stroh, R. Örlü, and D. Gatti. Flow resistance over heterogeneous roughness made of spanwise-alternating sandpaper strips. *Journal of Fluid Mechanics*, 980, Feb. 2024.

N. Hutchins, B. Ganapathisubramani, M. Schultz, and D. Pullin. Defining an equivalent homogeneous roughness length for turbulent boundary layers developing over patchy or heterogeneous surfaces. *Ocean Engineering*, 271: 113454, Mar. 2023.

J. Neuhauser, K. Schäfer, D. Gatti, and B. Frohnapfel. Simulation of turbulent flow over roughness strips. *Journal of Fluid Mechanics*, 945, July 2022.

L. von Deyn, D. Gatti, and B. Frohnapfel. From drag-reducing riblets to drag-increasing ridges. *Journal of Fluid Mechanics*, 951, Nov. 2022.

R. W. Zimmerman and G. S. Bodvarsson. Hydraulic conductivity of rock fractures. *Transport in porous media*, 23:1–30, 1996.